Sound scattering by rough elongated elastic objects. II: Fluctuations of scattered field

T. K. Stanton and D. Chu
Department of Applied Ocean Physics and Engineering, Woods Hole Oceanographic Institution, Woods Hole, Massachusetts 02543

(Received 8 June 1991; revised 10 April 1992; accepted 17 May 1992)

Sonar echoes from unresolved features of rough objects tend to interfere with each other. Because of these interferences, properties of the echoes, such as its envelope level, will vary from realization to realization of stochastically rough objects. In this article, the nature of the fluctuations of the backscattered echo envelope of rough solid elastic elongated objects is investigated. A general formulation is initially presented after which specific formulas are derived and numerically evaluated for straight finite-length cylinders. The study uses both the approximate modal-series- and Sommerfeld–Watson-transformation-based deformed cylinder solutions presented in the first part of this series [T. K. Stanton, J. Acoust. Soc. Am. **92**, 1641–1664 (1992)]. The fluctuations of the backscattered echo envelope are related to the Rice probability density function (PDF) and shown to depend upon σ/a and $\mathscr{L}/L$ in the Rayleigh scattering region ($ka \ll 1$) and $k\sigma$ and $\mathscr{L}/L$ in the geometric region ($ka \gg 1$), where σ is the rms roughness, a is the radius of the cylinder, $\mathscr{L}$ is the correlation length of the roughness, L is the length of the cylinder, and k is the acoustic wave number in the surrounding fluid. There are similarities shown between these fluctuations in the geometric region and those from rough planar interfaces. In addition, analytical expressions and numerical examples show that the fluctuation or "incoherent" component of the scattered field is random only in amplitude—its phase approaches a constant value, in phase with the mean scattered field, which needed to be taken into account in the formulation. Finally, applications of the theory developed in this article to backscatter data involving live marine shrimp-like organisms are discussed.

PACS numbers: 43.30.Ft, 43.30.Gv, 43.30.Hw

INTRODUCTION

Echoes from randomly rough objects will fluctuate from realization to realization. The fluctuations are due to the fact that there are interferences from the unresolved portions of the scatterer and the pattern of interferences is different in each realization, hence producing a different echo. The fluctuations depend upon the size, shape, orientation, and material properties of the object as well as the wavelength of the incident sound field. By understanding the physical basis of the fluctuations, one can make better predictions of the range of echoes in the "forward" sonar problem as well as make better estimates of the characteristics of the scatterer in the remote sensing, or "inverse" sonar problem.

In this second part of the series, the realization-to-realization fluctuations of the scattered field due to randomly rough straight finite elastic cylinders at normal incidence are investigated. Such variations are quite complex, especially when dealing with volumetric objects. What adds to the complexity of this problem over the subject of rough planar interface scattering is the fact that (1) circumnavigating surface elastic waves are present in the $ka \gg 1$ region and (2) in the $ka \ll 1$ (Rayleigh scattering) region, the fluctuations become functionally different than those in the $ka \gg 1$ region (where k is the wave number of the incident acoustic field and a is the radius of the cylinder). Neither of these two phenomena has a rough planar interface analog.[1]

The initial statistical formulas derived herein are general enough so that fluctuations due to other elongated bodies could also be predicted. The fluctuations of the level of the echo envelope are related to the Rice probability density function (PDF)[2] and the dependence of the PDF shape parameter γ upon the roughness properties of the cylinder is derived. Numerical examples involving Monte Carlo simulations of the approximate modal series solution are compared with the analytical results that were based on the modal series solution in the $ka \ll 1$ region and a simplified ray solution (an approximate form of the Sommerfeld–Watson transformed solution) in the $ka \gg 1$ region. Finally, applications of the analysis of the backscattered echoes from live marine shrimp-like organisms are discussed.

Finally, it is important to note that the fluctuations due to the stochastic nature of the rough boundary described in this article represent only one facet of a larger problem. Since the fluctuations also depend on other properties such as shape and orientation, which may be random, the fluctuations from all sources ultimately need to be taken into account to describe the echo statistics.

I. THEORY

In order to investigate the statistical nature of the echoes from randomly rough objects, we divide the analysis into

 0001-4966/92/091665-14$00.80

two major parts: (1) In the first part, the problem is purely statistical where the analogy between the stochastic acoustic scattering and the sum of an electrical sine wave and noise is made. The mean field of the acoustic echo is related to the constant amplitude sinusoidal (electrical) signal and the fluctuation component of the field is related to the noise component of the electrical signal. The Ricean probability density function (PDF),[2,3] which was originally derived in electrical signal theory, is then used to describe statistics of the echo envelope of the resultant sum of the acoustic "sine wave" and "noise". (2) In order to relate the statistical nature of the acoustic echo to the properties of the rough objects, the physics of the interaction of the sound waves and the objects must be understood. Here, we use the results of the previous article[1] where the scattering properties of the straight finite-length rough cylinder were derived. The acoustic "sine wave" and "noise" are derived from the mean and mean-square scattered field as was done in Stanton where the statistics of the scattering by rough planar interfaces were derived.[4] As it will be shown, there are additional degrees of complexity when dealing with volumetric objects because of the circumnavigating surface elastic waves in the $ka \gg 1$ region as well as Rayleigh scattering effects in the $ka \ll 1$ region.

A. Echo statistics (general)

The scattered pressure p_{scat}, due to one realization of a randomly rough object can be expressed in terms of the sum of the mean scattered pressure $\langle p_{\text{scat}} \rangle$ and the fluctuation component $p_{\text{scat}}^{(F)}$:

$$p_{\text{scat}} = \langle p_{\text{scat}} \rangle + p_{\text{scat}}^{(F)}, \tag{1}$$

where $\langle p_{\text{scat}}^{(F)} \rangle = 0$ and the brackets $\langle \cdots \rangle$ refer to an average across an ensemble of statistically independent objects. In the far field, where the pressure is proportional to the scattering amplitude f, we can write

$$f = \langle f \rangle + \delta f, \tag{2}$$

where $\langle \delta f \rangle = 0$ and now $\langle f \rangle$ is the mean field and δf is the fluctuation component. A phasor diagram of Eq. (2) is illustrated in Fig. 1. The mean field is also referred to as the coherent (or "stacked") component of the field in other articles as well as in this article. The time dependence of all quantities is suppressed.

Using Eq. (2), the mean-square scattering amplitude is

$$\langle ff^* \rangle = \langle f \rangle \langle f \rangle^* + \langle (\delta f)(\delta f)^* \rangle. \tag{3}$$

This equation can be rearranged to produce an equation for the mean-square fluctuation component of the scattered field:

$$\langle (\delta f)(\delta f)^* \rangle = \langle ff^* \rangle - \langle f \rangle \langle f \rangle^*. \tag{4}$$

As it will be shown in Sec. I B, the fluctuations of the echo envelope $|f|$ are directly related to the component δf_{in} of the (complex) fluctuation component that is in phase with the mean scattered field, especially when the roughness is small ($k\sigma \ll 1; |\delta f| \ll |f|$). In this region, the out-of-phase component $\delta f_{\perp}$ appears to have little affect on $|f|$ regardless of the relative values of δf_{in} and $\delta f_{\perp}$. One can understand this

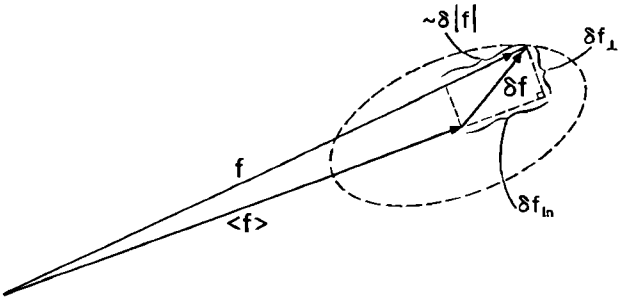

FIG. 1. Phasor representation of the scattering amplitude f shown to be the sum of two components: the mean field $\langle f \rangle$ and the fluctuation component of the field δf that has a zero mean. Also shown are the components of the fluctuation component that are in-phase (δf_{in}) and perpendicular ($\delta f_{\perp}$) or 90° out of phase with respect to the mean field. Fluctuations of the echo envelope are given by $\delta|f|$ and are approximately equal to δf_{in} for low fluctuations.

phenomenon qualitatively simply by examining the phasor diagram in Fig. 1 and seeing from a geometrical standpoint that changes of $\delta f_{\perp}$ will only cause minute changes in $|f|$. In particular, since f forms the hypotenuse of a right triangle in the complex plane, one can show that for small δf, changes in $|f|$ vary linearly with δf_{in} and quadratically with $\delta f_{\perp}$. Thus, to first order, δf_{in} alone causes variations in $|f|$ provided of course that $\delta f_{\perp}$ is not too much greater than δf_{in}.

It will be shown in later sections that the in-phase component becomes much greater than the out-of-phase component in two regions: the $ka \ll 1$ region and the low roughness ($k\sigma \ll 1$) high ka ($ka \gg 1$) scattering region. In each case, the phase of the fluctuation component approaches a narrow distribution in phase with the mean field. In these regions where $\delta f_{\text{in}} \gg \delta f_{\perp}$, variations of $|f|$ depend even less on $\delta f_{\perp}$ than had the two components been comparable.

For moderate roughness ($k\sigma \sim 1$) in the high ka region, the phase of the fluctuation component becomes uniformly distributed and $\delta f_{\text{in}} \sim \delta f_{\perp}$. In that case, either the in-phase or total fluctuation component can be used to describe the fluctuation of the echo envelope, although an analysis using the in-phase component only, even with a correction factor, decreases in accuracy.

Finally, in the Appendix, where the mean of the roughness was held at a nonzero level, it is shown that $\delta f_{\perp} \gg \delta f_{\text{in}}$. In that case, δf_{in} *still* dominated variations in $|f|$, which demonstrates again the importance of understanding the behavior of δf_{in} to describe the statistics of $|f|$.

We can write the in-phase component of the scattered field in terms of a vector or phasor dot product in the complex plane:

$$\delta f_{\text{in}} \equiv \frac{\delta f \cdot \langle f \rangle}{|\langle f \rangle|} = \frac{\text{Re}(\delta f)\text{Re}(\langle f \rangle) + \text{Im}(\delta f)\text{Im}(\langle f \rangle)}{\{[\text{Re}(\langle f \rangle)]^2 + [\text{Im}(\langle f \rangle)]^2\}^{1/2}}, \tag{5}$$

where the dot product ("·") between the fluctuation component and the normalized mean scattered field is first given symbolically and then written explicitly in terms of their

respective real and imaginary components. Note that δf_{in} is a real or "scalar" quantity.

The degree to which the level of the echo envelope fluctuates depends upon the relative values of the mean field and fluctuation component of the field (or, of course, in-phase component of the fluctuation component). When the fluctuation component is small compared with the mean field, the envelope fluctuates very little while conversely the fluctuations are great when the component is large compared with the mean. The fluctuations are small when the roughness is much smaller than an acoustic wavelength (or more precisely, $k\sigma \ll 1$). The fluctuations become large when $k\sigma \gtrsim 1$.

The ratio of the energies of the mean field to fluctuation (total or in-phase) component of the field determines the shape of the frequency distribution of the level of the echo envelope $|f|$:

$$\gamma_{\text{total}} \equiv \frac{\text{power of mean field}}{\text{power of } \textit{total} \text{ fluctuation component (uniform phase } \delta f \text{ only)}} = \frac{\langle f\rangle\langle f\rangle^*}{\langle ff^*\rangle - \langle f\rangle\langle f\rangle^*}, \tag{6}$$

$$\gamma_{\text{in}} \equiv \frac{\text{power of mean field}}{2(\text{power of } \textit{in-phase} \text{ fluctuation component})} = \frac{\langle f\rangle\langle f\rangle^*}{2\langle(\delta f_{\text{in}})^2\rangle}, \tag{7}$$

where the expression for $\langle(\delta f)(\delta f)^*\rangle$ in Eq. (4) was used in Eq. (6) and δf_{in} in Eq. (7) is defined in Eq. (5). Here, γ_{total} only applies when the phase of the fluctuation component is uniformly distributed $(0 - 2\pi)$ while γ_{in} can apply to the more general case when the phase is not uniform (so long as δf_{in} is not too much smaller than the out-of-phase component). The factor of 2 in the denominator of Eq. (7) was inserted to artificially produce what the total power of a *uniform* phase fluctuation component would be if the in-phase and out-of-phase components were equal. Later, γ_{in} will be used in the Rice distribution that was derived based on a uniform phase component whose total power *is* equal to twice one of its quadrature components.

The ratio γ is given above for the cases where the fluctuation of the echo envelope is determined by the total fluctuation component of the scattering amplitude in Eq. (6) and by the in-phase component of the fluctuation component in Eq. (7). These forms of γ can be used in the Rice PDF in a manner similar to that described in an earlier article involving scattering by rough planar interfaces:[4]

$$w(e) = \frac{2e(1+\gamma)}{\langle e^2\rangle} \exp\left(-\frac{(1+\gamma)e^2 + \gamma\langle e^2\rangle}{\langle e^2\rangle}\right) I_0(q'), \tag{8}$$

where

$$q' = \frac{2e[\gamma(1+\gamma)]^{1/2}}{\langle e^2\rangle^{1/2}},$$

$e(\equiv|f|)$ is the level of the echo envelope, and I_0 the modified Bessel function. Either γ_{total} or γ_{in} can be used in the γ term in Eq. (8). Note that there exists a more general form of the Rice PDF derived by Hoyt in which the two quadrature components, δf_{in} and $\delta f_{\perp}$, of the fluctuation component of the field are allowed to be unequal (they are assumed to be equal in the derivation of the Rice PDF).[5] While applying the Hoyt PDF to the current problem would be more rigorous, we have found that our adaptation of the Rice parameter γ to γ_{in} to be not only mathematically convenient but it allows the Rice PDF to satisfactorily describe the echo fluctuations over a wide range of conditions without sacrifice of accuracy (Secs. II and III).

Figure 2 gives examples of the Rice PDF for various values of γ. For $\gamma = 0$, the Rice PDF becomes the Rayleigh PDF. This occurs, as shown in Eqs. (6) and (7), when the echo is dominated by the fluctuations due to the roughness and the echo will fluctuate as would pure noise. That is, the surface of the object is so rough that there is a negligible coherent return and the echo fluctuates significantly. When the cylinder becomes acoustically smooth, the coherent or mean component of the echo dominates ($\gamma \gg 1$) and the PDF tends to a narrow Gaussian. In this case, the echo fluctuates very little. For intermediate roughnesses, the PDF takes on intermediate curves. The Rice PDF varies smoothly between the extremes. The fluctuations of the echo amplitude will be related to physical scattering processes in Sec. I B.

B. Relating scattering by rough cylinders to echo statistics

As shown in Sec. I A, the statistical nature of the echo envelope of a rough object is related to the mean and mean-square scattered fields. Derivation of explicit analytical expressions requires dividing the analysis into two subsections: (1) the $ka \ll 1$ region, where the modal series solution is used as the series simplifies to the summation of the first two modal terms (a monopole and dipolelike term) which dominate the scattering process; (2) the $ka \gg 1$ region, where a simpli-

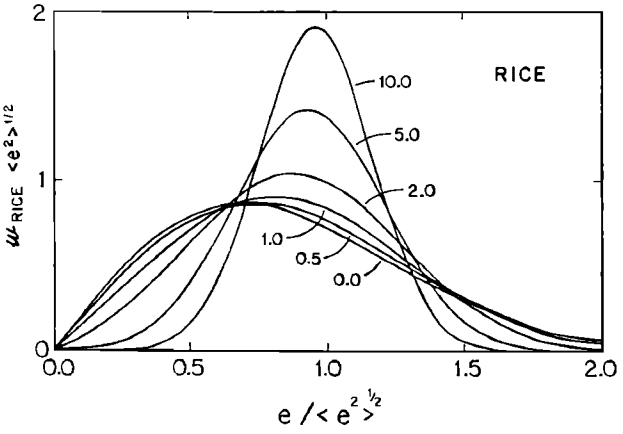

FIG. 2. Rice PDF of the envelope level for various values of γ. The $\gamma = 0$ curve is the Rayleigh PDF where the fluctuating component of the echo dominates the echo envelope (mean component of scattering amplitude is zero). As γ becomes large, the mean component dominates and the PDF approaches the Gaussian.

fied ray solution based on the Sommerfeld–Watson transformation (SWT) of the modal series is used (in this region, the modal series requires many terms to converge and is difficult, if not impossible, to manipulate mathematically). Both solutions, involving the deformed cylinder formulation, are approximate.

1. $ka \ll 1$

The $ka \ll 1$ expansion to the approximate modal-series-based backscattering amplitude for the straight finite rough cylinder was given in Ref. 1 as

$$f_{RC} \simeq f_0 + \frac{1}{2}\alpha_\pi \int_{-L/2}^{L/2} (k\zeta)^2\, dz = f_0\left[1 + L^{-1}\int_{-L/2}^{L/2}\left(\frac{\zeta}{a}\right)^2 dz\right], \tag{9}$$

where $f_0 \equiv \frac{1}{2}\alpha_\pi (ka)^2 L$ and is the zero roughness scattering amplitude for $ka \ll 1$, $\alpha_\pi \equiv (1 - gh^2)/2gh^2 + (1-g)/(1+g)$, g and h are the density and compressional speed of sound contrasts of the material, k is the acoustic wave number of the surrounding fluid, ζ is the roughness deviation about the mean radius a of the cylinder, z is the position along the axis of the cylinder, L is the length of the cylinder, and $\int_{-L/2}^{L/2}\zeta\, dz = 0$ was assumed. The above equation is characterized by two terms—the first is the scattering amplitude in the absence of roughness while the second represents changes in the amplitude due to roughness. Since ζ is stochastic, so is the scattering amplitude.

The mean scattering amplitude is simply

$$\langle f_{RC}\rangle = f_0\left[1 + L^{-1}\int_{-L/2}^{L/2}\left\langle\left(\frac{\zeta}{a}\right)^2\right\rangle dz\right], \tag{10}$$

where the brackets $\langle\cdots\rangle$ represent an average over an ensemble of statistically independent cylinders. The fluctuation component, as defined in Eq. (2), can be determined from the above two equations as

$$\delta f = f_0 L^{-1}\int_{-L/2}^{L/2}\left[\left(\frac{\zeta}{a}\right)^2 - \left\langle\left(\frac{\zeta}{a}\right)^2\right\rangle\right] dz \tag{11a}$$

$$= f_0 L^{-1}\int_{-L/2}^{L/2}\left[\left(\frac{\zeta}{a}\right)^2 - \left(\frac{\sigma}{a}\right)^2\right] dz, \tag{11b}$$

where the rms roughness $\sigma \equiv \langle\zeta^2\rangle^{1/2}$ was substituted in Eq. (11b).

In order to predict fluctuations in the levels of the echo envelope, we must now examine the phase characteristics of the fluctuation component of the scattering amplitude. The above equations show that, to first order, both the mean scattered field and fluctuation component are real, hence in phase with each other. Determination of the in-phase component of the fluctuation as given in Eq. (5) is then trivial as $\langle f\rangle = |\langle f\rangle|$, which makes $\delta f_{in} = \delta f$. Determination of γ_{in} in Eq. (7) is straight forward as we now use Eq. (11b) to calculate the mean square of the in-phase component. First, the square is written:

$$(\delta f_{in})^2 = f_0^2 L^{-2}\int_{-L/2}^{L/2}\int_{-L/2}^{L/2}\left[\left(\frac{\zeta'}{a}\right)^2\left(\frac{\zeta''}{a}\right)^2 - 2\left(\frac{\sigma}{a}\right)^2\left(\frac{\zeta'}{a}\right)^2 + \left(\frac{\sigma}{a}\right)^4\right] dz'\, dz'', \tag{12}$$

where the prime(s) on each ζ indicate to which z integration it belongs. Without making any assumptions with regard to the statistical nature of ζ, this expression shows that the square of the in-phase fluctuation component varies as the fourth power of roughness which, in turn, results in γ_{in} varying *inversely* upon the fourth power of roughness.

Taking the mean of the above equation involves knowledge of the statistical behavior of ζ. Assuming that ζ is Gaussian distributed about a zero mean, this equation can readily be evaluated analytically. Note that since the first term in the integrand involves two variables, ζ' and ζ'', the bivariate Gaussian distribution is required. Using the results of the averages $\langle\zeta'^2\rangle$ and $\langle\zeta'^2\zeta''^2\rangle$ given in Appendix A of Ref. 1, the mean square in-phase fluctuation component is

$$\langle(\delta f_{in})^2\rangle = 2f_0^2\left(\frac{\sigma}{a}\right)^4 L^{-2}\int_{-L/2}^{L/2}\int_{-L/2}^{L/2}\Phi^2(\xi)\, dz'\, dz'', \tag{13}$$

where the factor to the zero roughness term in the mean square is shown to depend upon the product of the fourth power of roughness, twofold integral of the square of the autocorrelation function of the surface, and the correlation parameter $\xi = z'' - z'$. Further evaluation of the mean square requires knowledge of the autocorrelation function. In Appendix B of Ref. 1, an estimate of the integral was made assuming a simple function that decreased linearly to zero from the origin and remained equal to zero beyond that point which was defined as the "correlation length" $\mathscr{L}$. Replacing the integral with its estimated value of (2/3) $\mathscr{L}L$ gives

$$\langle(\delta f_{in})^2\rangle \simeq \frac{4}{3}f_0^2\left(\frac{\sigma}{a}\right)^4\frac{\mathscr{L}}{L}, \tag{14}$$

where the relation $\mathscr{L}/L \ll 1$ was assumed in evaluating the integral. (This is a practical assumption because if the correlation length were comparable to or greater than L, then the object would not be rough.)

Inserting Eqs. (10) and (13) into Eq. (7) gives expressions for γ_{in}:

$$\gamma_{in} = \left[1 + \left(\frac{\sigma}{a}\right)^2\right]^2\left[4\left(\frac{\sigma}{a}\right)^4 L^{-2}\int_{-L/2}^{L/2}\int_{-L/2}^{L/2}\Phi^2(\xi) \times dz'\, dz''\right]^{-1} \tag{15a}$$

$$\simeq \left[4\left(\frac{\sigma}{a}\right)^4 L^{-2}\int_{-L/2}^{L/2}\int_{L/2}^{L/2}\Phi^2(\xi)\, dz'\, dz''\right]^{-1} \tag{15b}$$

$$\simeq \left[\frac{8}{3}\left(\frac{\sigma}{a}\right)^4\frac{\mathscr{L}}{L}\right]^{-1}, \tag{15c}$$

where the integral of the mean-square roughness in Eq. (10) was evaluated to produce Eq. (15a), (σ/a) was assumed to be much less than unity in the approximation in Eq. (15b), and the approximate expression for the integral of the corre-

lation function as discussed above was inserted into Eq. (15b) to produce Eq. (15c).

The above expressions for γ_{in} show that for $ka \ll 1$, the behavior of the fluctuations of the echo envelope is independent of frequency and only depends on the roughness parameters. In addition, although Eq. (15a) was derived for $ka \ll 1$, the only restriction on the roughness is that it is slowly varying. The roughness is thus allowed to be finite in magnitude (compared with a).

The fact that the echo fluctuations are independent of frequency in the $ka \ll 1$ region for the entire range of roughness is a phenomenon that is specific to volumetric scattering and should be compared with fluctuations due to rough planar interfaces where the fluctuations can depend directly upon frequency. In the case of rough planar interfaces, Stanton showed that γ varied by an inverse power of k in the low roughness ($k\sigma \ll 1$) case.[4] Once $k\sigma$ became much greater than unity, the fluctuations were Rayleigh distributed and were not sensitive to changes in frequency. The underlying reason for the above differences is the fact that for $ka \ll 1$, the variations in the scattering amplitude are caused by variations in the *amplitude* of the "local" echo from the infinitesimal slice of the cylinder that is integrated while phase-shift-induced fluctuations are negligible [Eq. (9)]. The mathematics show that this amplitude-variation-induced fluctuation, normalized by the mean, is independent of frequency. In contrast, for the planar interface variations are due to local changes in *phase* while the local changes in amplitude are quite often considered negligible. The phase shifts are frequency dependent, hence resulting in the frequency dependence of the fluctuations for rough planar interfaces.

Finally, in a manner similar to the above discussion, subsection B 2 illustrates the same types of differences between the fluctuations due to a rough cylinder at $ka \ll 1$ and $ka \gg 1$.

2. $ka \gg 1$

The backscattering amplitude as derived with a simplified ray solution [an approximate form of the Sommerfeld–Watson-transformed (SWT) solution] for rough solid elastic finite cylinders was given in Ref. 1 as

$$f_{RC} \simeq \frac{-i}{2\sqrt{\pi}} e^{i\pi/4} \int_{-L/2}^{L/2} \times \Big(\mathscr{R} e^{-i2k[a+\zeta(z)]} \sqrt{k[a+\zeta(z)]} - 8\sqrt{\pi} k[a+\zeta(z)] \beta'_R(\infty) e^{i\Phi_R} \exp\{-2(\pi-\theta_R)k[a+\zeta(z)]\beta'_R(\infty)\} \times \exp\{ik[a+\zeta(z)][(c/c_R)(2\pi-2\theta_R)-2\cos\theta_R]\} \times \sum_{m=0}^{\infty} \exp\{-2\pi m k[a+\zeta(z)]\beta'_R(\infty)\} \exp\{i2\pi m k[a+\zeta(z)]c/c_R\} \Big) dz, \tag{16}$$

where $\mathscr{R} \equiv (gh-1)/(gh+1)$ is the plane-wave/plane interface reflection coefficient.

The first term in the integrand of this ray solution is the so-called "specular" echo from the front interface of the cylinder and the second term represents the Rayleigh surface elastic waves that have circumnavigated the cylinder and returned toward the source. It was shown, in part, in Ref. 1 and more completely in Refs. 6–9 that the specular echo and Rayleigh surface waves dominate the trend and oscillatory nature of the backscattering by certain dense elastic bodies when plotted versus ka while waves such as the Franz, Whispering Gallery, and internally refracted waves that were ignored in the analysis in Ref. 1 could be ignored in the $20 < ka < 80$ range. The definitions for the Rayleigh wave parameters are given in Ref. 1 and will not be repeated here because, as explained below, the Rayleigh wave will be ignored in the analysis. Also, there are several major assumptions leading to Eq. (16) including the requirement that the radius vary slowly with z and the fact that dispersion of the Rayleigh wave is ignored. Since the Rayleigh wave is ignored in this analysis, the latter assumption is irrelevant to this article.

Formulating the behavior of the echo fluctuations using the above equation would be extremely difficult because of the Rayleigh wave component. In order to illustrate the underlying physical phenomena and general trends involved in the fluctuations of the echo envelope, we ignore the Rayleigh surface wave component and examine only the specular wave. This can be justified because, as shown in Ref. 1, the specular wave dominated the trend of the scattering over a large range of ka [at very high ka, the Rayleigh wave component will dominate the scattering by (one dimensional) rough objects]. The assumption will be further verified later in this article when the simplified theory is compared with numerical simulations that include all surface waves. Ignoring the Rayleigh term and rewriting the specular term, the above equation simplifies to

$$f_{RC} = f_0 L^{-1} \int_{-L/2}^{L/2} e^{-i2k\zeta} \sqrt{1+\frac{\zeta}{a}}\, dz, \tag{17}$$

where $f_0 \equiv -(i/2\sqrt{\pi}) e^{i\pi/4} \mathscr{R} e^{-i2ka} \sqrt{ka} L$ is the zero roughness scattering amplitude for $ka \gg 1$.

The integrand in Eq. (17) contains the product of two terms—one whose phase varies with roughness and the other whose amplitude varies with roughness. The problem that will be investigated involves roughness that is low both with respect to the wavelength of the incident sound ($k\sigma \ll 1$) and radius of the cylinder ($\sigma/a \ll 1$). In the $k\sigma \ll 1$ region, the shape of the (narrow) probability density function of the echo envelope will be shown to contain much information regarding the roughness properties of the object. This is in contrast to the $k\sigma \gtrsim 1$ region where the envelopes are Ray-

leigh distributed and much less information is extractable from the envelope distribution. The $\sigma/a \ll 1$ condition is imposed because if σ were comparable to or greater than the radius, the cylinder would break.

It is also important to note that for $\zeta/a \ll 1$, the square root term in Eq. (17) is approximately unity and f_{RC} broadly resembles the scattering in the specular direction by a one-dimensional rough planar interface (with the assumption of small slopes).[10-12] Thus the results of the analysis about to be presented also apply, at least qualitatively, to the rough planar interface problem.

In the low roughness limit, the expansions $e^{-i2k\zeta} \simeq 1 - i2k\zeta - 2(k\zeta)^2$ and $\sqrt{1+\zeta/a} \simeq 1 + \frac{1}{2}\zeta/a - \frac{1}{8}(\zeta/a)^2$ are used in the above equation to obtain the approximation expression

$$f_{RC} \simeq f_0\left[1 - 2L^{-1}(ka)^2 \int_{-L/2}^{L/2}\left(\frac{\zeta}{a}\right)^2 dz - iL^{-1}(ka)\int_{-L/2}^{L/2}\left(\frac{\zeta}{a}\right)^2 dz\right], \tag{18}$$

where the roughness was assumed to have a zero mean along the length ($\int_{-L/2}^{L/2}\zeta\, dz = 0$). This equation shows that the scattering amplitude has orthogonal components to it, the first two being 90° out of phase in the complex plane from the third (note that f_0 is complex). The third term is also of a lower order of ka than the second and will be shown to have a negligible effect on the echo fluctuations.

The mean scattering amplitude is determined from the above equation as

$$\langle f_{RC}\rangle = f_0[1 - 2(ka)^2(\sigma/a)^2 - i(ka)(\sigma/a)^2] \tag{19}$$

and, using the above two equations, the fluctuation component is

$$\delta f = f_0\left\{2L^{-1}(ka)^2\int_{-L/2}^{L/2}\left[\left(\frac{\sigma}{a}\right)^2 - \left(\frac{\zeta}{a}\right)^2\right]dz + iL^{-1}(ka)\int_{-L/2}^{L/2}\left[\left(\frac{\sigma}{a}\right)^2 - \left(\frac{\zeta}{a}\right)^2\right]dz\right\}. \tag{20}$$

The in-phase fluctuation component can be calculated formally by use of Eq. (5) or by simple inspection of Eq. (20). Either way the in-phase component is found to be equal to the product of f_0 and the first term in the brackets in Eq. (20):

$$\delta f_{in} \simeq 2|f_0|L^{-1}(ka)^2\int_{-L/2}^{L/2}\left[\left(\frac{\sigma}{a}\right)^2 - \left(\frac{\zeta}{a}\right)^2\right]dz. \tag{21}$$

It is important to point out that, as in the $ka \ll 1$ case, the in-phase component dominates the fluctuation component as indicated by the fact that the real term in the brackets in Eq. (20) is much greater than the imaginary term for $ka \gg 1$ [the higher-order terms representing the out-of-phase components in Eqs. (9) and (11) were not shown as they were negligible]. Thus in both regions, the fluctuations of the scattering amplitude are essentially in phase with the mean scattered field.

Using the above equation, the square of the in-phase fluctuation component is

$$(\delta f_{in})^2 = 4|f_0|^2 L^{\ 2}(ka)^4\int_{-L/2}^{L/2}\int_{-L/2}^{L/2}\left[\left(\frac{\sigma}{a}\right)^4 - 2\left(\frac{\zeta'}{a}\right)^2\left(\frac{\sigma}{a}\right)^2 + \left(\frac{\zeta'}{a}\right)^2\left(\frac{\zeta''}{a}\right)^2\right]dz'\,dz''. \tag{22}$$

As we observed in the $ka \ll 1$ case [Eq. (12)], without making any assumptions about the statistical nature of the roughness, the mean square of this component varies with the fourth power of the roughness indicating that γ_{in} will vary *inversely* with the fourth power of roughness. As in the analysis involving the $ka \ll 1$ case, we proceed by assuming the roughness to be Gaussian distributed about a zero mean. Performing the mean of the above equation and using the results of the averages $\langle\zeta'^2\rangle$ and $\langle\zeta'^2\zeta''^2\rangle$ given in Appendix A of Ref. 1,

$$\langle(\delta f_{in})^2\rangle = 8|f_0|^2 L^{-2}(ka)^4\left(\frac{\sigma}{a}\right)^4 \times\int_{-L/2}^{L/2}\int_{-L/2}^{L/2}\Phi^2(\xi)dz'\,dz'', \tag{23}$$

where the factor to the zero roughness term is shown to depend upon the fourth power of both k and σ, which is in contrast to the $ka \ll 1$ case where there was no k dependence in the corresponding factor ($|f_0|^2$, of course, depends upon k in each case). In both cases, the component depends upon the same integral of the square of the autocorrelation function.

As in the $ka \ll 1$ analysis, we use the estimate of the integral involving the correlation function given in Appendix B of Ref. 1 to produce an approximate explicit expression for the above equation

$$\langle(\delta f_{in})^2\rangle \simeq \tfrac{16}{3}|f_0|^2(ka)^4\left(\frac{\sigma}{a}\right)^4\frac{\mathscr{L}}{L}, \tag{24}$$

where the value $(2/3)\mathscr{L}L$ was substituted for the integral. Inserting Eqs. (19) (low roughness limit), (23), and (24) into Eq. (7) gives

$$\gamma_{in} = \left[16(ka)^4\left(\frac{\sigma}{a}\right)^4 L^{-2}\int_{-L/2}^{L/2}\int_{-L/2}^{L/2}\Phi^2(\xi)dz'\,dz''\right]^{-1} \tag{25}$$

$$\simeq\left[\frac{32}{3}(ka)^4\left(\frac{\sigma}{a}\right)^4\frac{\mathscr{L}}{L}\right]^{-1}. \tag{26}$$

Combining the $(ka)(\sigma/a)$ products above, we obtain

$$\gamma_{in} = \left(16(k\sigma)^4 L^{-2}\int_{-L/2}^{L/2}\int_{-L/2}^{L/2}\Phi^2(\xi)dz'\,dz''\right)^{-1} \tag{27}$$

$$\simeq\left(\frac{32}{3}(k\sigma)^4\frac{\mathscr{L}}{L}\right)^{-1}. \tag{28}$$

We show both forms of the above two pairs of equations with the $k\sigma$ and $(ka)(\sigma/a)$ products to help illustrate the various dependences of $k\sigma$, ka (σ/a fixed), and σ/a (ka fixed). Discussions and numerical simulations will involve some or all combinations.

The above equations for γ [Eqs. (25)–(28)] show that the relative echo envelope fluctuations depend upon both k and σ. This is in contrast to the $ka \ll 1$ case where the fluctu-

ations did not depend upon k (see Table I for summary). In both cases, γ_{in} varies inversely as the fourth power of roughness. Note also that, as shown in Ref. 4, for $k\sigma \ll 1$ the echoes from a rough planar interface vary with both k and σ as do the echoes for the $k\sigma \ll 1$, $ka \gg 1$ case with the rough cylinders. These above differences and similarities are due to the differences in the scattering processes arising between volumetric and planar interfaces. For $ka \ll 1$ in the cylinder case, the object is monopole- and dipolelike and exhibits scattering properties for which there are no counterparts in the scattering by continuously rough planar interfaces. In the $ka \gg 1$ region, the scattered field due to the cylinder can be reasonably described by rays and there are strong similarities between the scattering by the cylinders and planar interfaces.

II. NUMERICAL EXAMPLES

In this section, we examine the fluctuations of the echo envelope that occur from realization to realization due to a plane wave normally incident upon randomly rough straight finite-length elastic (tungsten carbide) cylinders. Many realizations of the rough surface of the cylinder were involved allowing us to compare the Rice PDF with histograms of the echo envelope as well as investigate the characteristics of the fluctuation component itself with respect to its phase and amplitude. The scattering by the statistical ensembles of the cylinders was calculated for both the cases of (1) holding the rms roughness fixed while varying ka and (2) holding ka fixed while varying the rms roughness. In case (1), the variations in the nature of the fluctuations due to modal interferences are illustrated and in case (2) the similarity between the scattering by the cylinder and a rough planar interface is illustrated.

Figure 3 is a plot of the normalized scattering amplitude versus ka for a smooth tungsten carbide straight finite-length cylinder at normal incidence. The scattering can be characterized by two regions: (1) in the $ka \ll 1$ or Rayleigh scattering region, the wavelength is much larger than the radius of the cylinder that exhibits monopole and dipolelike behavior. In this region, the scattering increases rapidly, smoothly, and monotonically with ka until approximately $ka = 1$ where a transition into geometric scattering occurs. (2) In the $ka \gg 1$ or geometric scattering region, the wavelength is much smaller than the radius of the cylinder and the incident waves of sound interact with the cylinder like rays. The oscillatory behavior of the scattering curve versus ka is due to interferences between the wave that is "specularly reflected" off the front interface of the cylinder, the surface waves that are reradiated back toward the receiver, and internally refracted and reradiated waves. The dominant waves in the upper ka region of this plot are the specular and Rayleigh surface elastic waves where the specular wave dominates the trend of the scattering while the interference

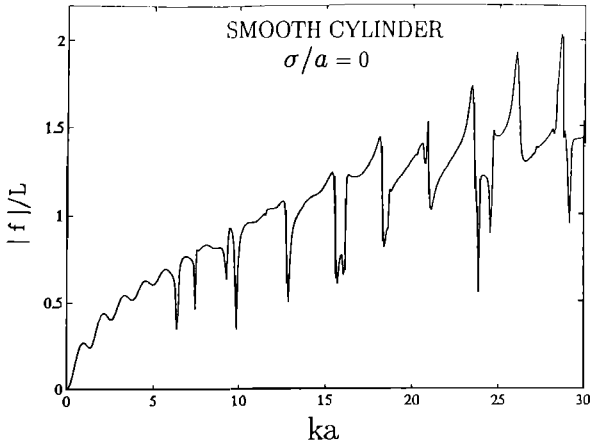

FIG. 3. Scattering amplitude (absolute value) or echo envelope, normalized by length of cylinder, of smooth (zero roughness) finite-length tungsten carbide (elastic) cylinder at broadside incidence versus ka. The modal series solution (converged using first 36 terms) was used in the approximate finite cylinder formulation. Illustrated are the Rayleigh scattering region ($ka \ll 1$) where the curve rises rapidly and monotonically and the geometric scattering region ($ka > 1$) where the curve increases less rapidly and experiences oscillations about a trend due to interferences between the specular, surface wave, and internally refracted components of the scattered field. For equations and material properties used, see Refs. 13 and 1.

TABLE I. Comparison between the zero roughness backscattering cross section and properties of fluctuations of echo envelope due to rough cylinders for Rayleigh ($ka \ll 1$) and geometric ($ka \gg 1$) scattering regions. By the definition used in this article, $\sigma_{bs} \equiv |f|^2$ and TS $= 10 \log \sigma_{bs}$, where TS is target strength.

SMOOTH		ROUGH		
ka	Backscattering cross section σ_{bs}	$k\sigma$	Phase distribution of fluctuation component of scattered field	Rice PDF shape parameter γ
$ka \ll 1$	$\frac{1}{4}a_\pi^2 (ka)^4 L^2$	$k\sigma \ll 1$	narrow, in phase with $\langle f \rangle$	$\left\{4\left(\frac{\sigma}{a}\right)^4 L^{-2} \int_{-L/2}^{L/2}\int_{-L/2}^{L/2} \Phi^2(\xi)\,dz'\,dz''\right\}^{-1}$
$ka \gg 1$	$(1/4\pi)\mathscr{R}^2 kaL^2$	$k\sigma \ll 1$	narrow, in phase with $\langle f \rangle$	$\left\{16(k\sigma)^4 L^{-2} \int_{-L/2}^{L/2}\int_{-L/2}^{L/2} \Phi^2(\xi)\,dz'\,dz''\right\}^{-1}$
		$k\sigma \gtrsim 1$	uniform	near 0 independent of k, σ, Φ

between it and the Rayleigh waves causes the major oscillations.[6-9]

In order to simulate the scattering by randomly rough cylinders, the radius of the cylinder in the deformed cylinder formulation was randomized with respect to position along the axis (i.e., the radius function was, in the analogy to electrical signal theory, a "time series" of "bandlimited noise" along the axis). Each surface was constructed so that its radius was Gaussian distributed about its mean value. The surfaces and the use of them in the deformed cylinder formulation are discussed in detail in the previous article.[1]

Figure 4 illustrates variations in the magnitude of the scattering amplitude (echo envelope) of randomly rough tungsten carbide cylinders. Plotted in Fig. 4(a) and (b) are the value of the magnitude of the scattering amplitude (normalized by L) for each realization at each value of ka as calculated by the approximate modal-series based solution. For every value of ka, there were 300 realizations of $|f|/L$ calculated, although due to memory limitations of our printer only 150 of those points were shown in Fig. 4(a) and (b). The calculations were performed with two roughnesses—$\sigma/a = 0.01$ in Fig. 4(a) and $\sigma/a = 0.05$ in Fig. 4(b). Echo envelope histograms (now involving all 300 realizations per value of ka) and associated Rice PDF curves for several sets of realizations are given in Fig. 4(c).

All plots in Fig. 4 illustrate that for low roughness ($k\sigma \lesssim 0.5$), the relative fluctuations or spread of points are small while for higher values of $k\sigma$, the fluctuations are great. [The theoretical transition point $k\sigma = 0.5$ occurs at $ka = 50$ and 10 for $\sigma/a = 0.01$ and 0.05, respectively. Figure 4(a) does not show the transition point as all ka values are below 30.] In terms of the acoustic wavelength, when the roughness is much smaller than the wavelength (or more precisely the *reduced* wavelength, $\lambda/2\pi$) the effects due to roughness and hence fluctuations are smaller. Conversely, for the case where the roughness is much greater than λ, the fluctuations are great. These plots should also be compared with Figs. 9–11 of the previous article where the mean and mean square of the scattering amplitude are shown to decrease due to roughness effects beyond the $k\sigma = 0.5$ point. The decrease of the means is indicative of the increase in fluctuations.

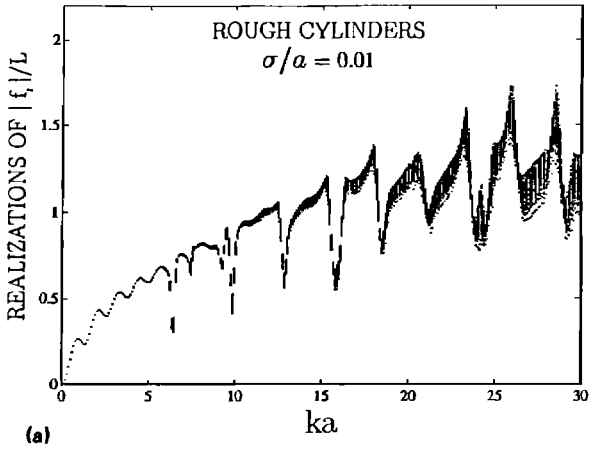

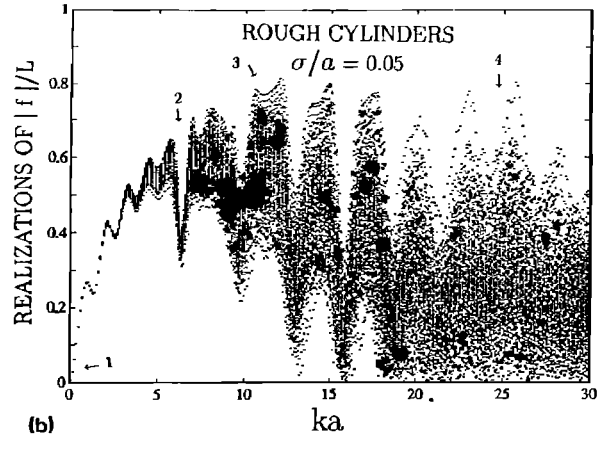

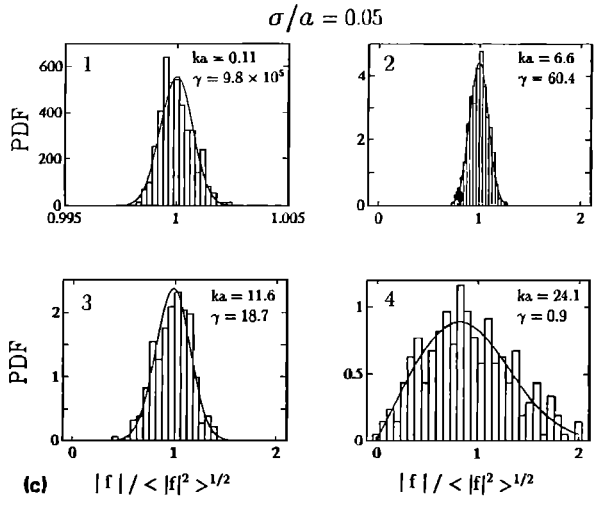

FIG. 4. (a) Plot of the normalized magnitude of the scattering amplitude or echo envelope $|f|/L$, for 150 realizations of roughness ($\sigma/a = 0.01$) for the randomly rough finite-length tungsten carbide cylinder at broadside incidence versus ka. $|f|/L$ is plotted for each realization producing a "scatter pattern" of points for each value of ka where a is the mean radius of each rough cylinder. The modal series solution (converged using first 36 terms) was used in the (approximate) deformed cylinder formulation as applied to the rough cylinder case described in Ref. 1. The calculations were performed in the same manner as in Fig. 10 of Ref. 1 but with 150 realizations. (b) Same as (a) but for $\sigma/a = 0.05$. Arrows indicate positions where histograms [shown in (c)] are calculated. (c) Histograms of the levels of echo envelopes from (b) and realizations not shown at several ka values with Rice PDFs superimposed (Rice shape parameter, γ, is given in plot). Three-hundred realizations per value of ka were used to form the histograms. The plots are numbered (upper left-hand corner) to correspond to the $|f|/L$ values denoted by arrows in (b). All plots in Fig. 4 show the relative fluctuations to be small in the $k\sigma < 0.5$ region, which corresponds to low roughness [$ka < 50$ (i.e., all values of ka shown) in (a) and $ka < 10$ in (b)]. The relative fluctuations are large in the $k\sigma > 0.5$ or high roughness region. The plots in (c) also illustrate the degree to which the Rice PDF describes the distribution of echo values.

The good fits between the theoretical Rice PDF and the histograms shown verify that the fluctuations are approximately Ricean distributed. We compared the Rice PDF with histograms at each value of ka and found the comparison or "goodness of fit" to be similar to the fits shown in this figure for most cases. There were some histograms that contained some skew not predicted by the Ricean function. The presence of nulls may explain the skew. The values of γ derived by fits to the histograms were not significantly affected by the skew.

The histograms show that for the lowest values of ka (where $k\sigma \ll 1$) the PDF is narrow and Gaussianlike (high γ) indicating that the fluctuation in this acoustically smooth region is small compared with the level of the envelope. As ka is increased and hence the surface becomes acoustically rougher, the degree of fluctuation increases and the PDFs broaden accordingly until they approach the Rayleigh PDF ($\gamma = 0$).

For this entire analysis presented in this section, the observed or true Rice PDF parameter, γ, was determined by computer algorithm: for $\gamma \geqslant 10$, since the Rice PDF rapidly approaches the characteristics of the Gaussian PDF, we used the simple formula $\gamma = (\langle e^2 \rangle)/(2\sigma_e^2)$, where $\langle e^2 \rangle$ is the mean square of the echo envelope and σ_e is the standard deviation of the distribution of the echo envelope. For $\gamma < 10$, there was no simple formula to use and the computer iteratively fit many Rice PDFs to each distribution involving a range of closely spaced values of γ (0.1 increments) until the "best" (least-squares) fit was obtained. The observed γ will be compared with calculated values of γ_{in} based on simulation values of $\langle f \rangle$ and δf_{in} [Eqs. (5) and (7)] and values based on the low roughness theories given in Eqs. (15b) and (25).

We summarize the fluctuations in Fig. 4 by plotting the Rice PDF shape parameter γ versus ka on a log–log scale in Fig. 5. As predicted in Sec. I, there are three different regions of fluctuation phenomena—one in the $ka \ll 1$ (Rayleigh) scattering region where the fluctuations are small (high γ) and do not depend upon the wave number k, the second in the $ka \gg 1$ (geometric scattering) but low roughness ($k\sigma \ll 1$) region where the fluctuations are small (high γ) and depend strongly on $k(\gamma \sim k^{-4})$, and the third in the $ka \gg 1$ but high roughness ($k\sigma > 1$) region where the fluctuations are large (low γ) and do not depend strongly on k [i.e., in this limit of very high frequency, the phases of all wavelets are random ($0 - 2\pi$) and the fluctuations cannot increase further]. The dashed lines are based on low roughness theories presented earlier in this article for the $ka \ll 1 (\sigma/a \ll 1)$ and $ka \gg 1 (k\sigma \ll 1, \sigma/a \ll 1)$ regions.

There is excellent agreement between the theory and simulations in the $ka \ll 1$ region while in the low roughness portion of the $ka \gtrsim 1$ region there is agreement between the general *trends*, but not the structure. In general, the solid curves based on the simulations in the $ka \gtrsim 1$ region are shown to have a complex structure whose trend decreases as $(ka)^{-4}$ as predicted by the simple theory, but with downward dips or spikes whose positions correspond more or less with the positions of the nulls in the backscatter versus ka plot for smooth cylinders in Fig. 3. The discrepancy between the theory and simulations is quite obviously due to the fact that the simple theory involved only the specular component and did not take into account the fact that interferences between the specular echo with other waves such as the Franz and Rayleigh waves also contribute to the fluctuations. In the $ka \ll 1$ region, the theory incorporated all dominant mechanisms (monopole and dipole terms) which explains the better fit in that region. The peak at $ka \simeq 0.5$ occurs in the

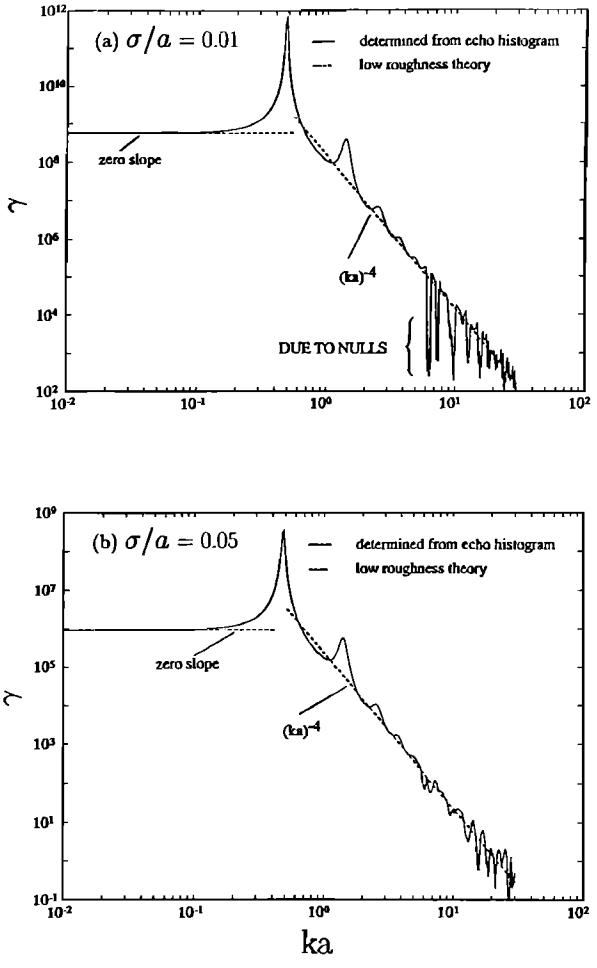

FIG. 5. Solid: Rice PDF shape parameter γ plotted against ka from the distributions of echo envelope shown in Fig. 4(a) and (b). As in Fig. 4(c) 300 realizations per value of ka were used to determine γ. The dashed lines are from calculations of the low roughness ($k\sigma \ll 1$) theories for γ in the text [Eq. (15b) for $ka \ll 1$ and Eq. (25) for $ka \gg 1$]. The integral of the square of the correlation functions in the equations was calculated numerically from the rough surfaces. The parameter γ is shown to be constant (independent of the wave number k) in the $ka \ll 1$ Rayleigh scattering region and decrease rapidly with increasing ka in the $ka > 1$ region. The deviations from the trend in the rapidly decreasing section indicate the sensitivity of γ to the nulls in the backscatter versus ka plot illustrated in Fig. 3. The position of the dips in these plots of γ correspond to the position of the nulls in Fig. 3. The dips are deeper for the low roughness case because more local radius values at these positions will be distributed along the steep "walls" of the null than in the higher roughness case, hence causing greater variability of the echo. The theory, which predicts a smooth variation in γ for $ka \gg 1$ includes only the specular component of the scattering and hence ignores all interference effects involving other types of waves. The values of γ were calculated from the variance of $|f|$ for $\gamma \geqslant 10$ since the Rice PDF resembles a Gaussian in that region and least squares fits of the PDF to the distribution of $|f|$ for $\gamma < 10$.

complicated transition zone between Rayleigh and geometric scattering and is not explained by the low or high ka solutions. It does not correspond to any peaks or nulls in the $|f|/L$ vs ka plot for smooth cylinders.

The increase in fluctuations (local minimum in γ) at the null points can be explained as follows: If the product of mean radius and wave number has a value that is at or near a null point, then small variations in the radius along the length of the cylinder will cause the value of ka to move within the null region causing large variations in value of scattering amplitude of the "local" echo due to the infinitesimal slices of the cylinder. The resultant total echo from all slices then has increased fluctuations over what it would have without the presence of the null. The variability of γ due to this effect is more pronounced in the lower roughness case because the distribution of values of local radii will be narrower, hence there will be a larger percentage of sections of the cylinder that will be experiencing the null effect. For larger roughness, the radii will have a wider distribution and at any given null point, a substantial fraction of radii will be outside the range of values that would cause a null thus reducing its effect on the fluctuations.

In order to separate effects between fluctuations due to scattering of the specular wave off the front interface and the fluctuations discussed above due to the presence of nulls, we continue the analysis by now holding ka fixed while varying the rms roughness. The simulations in the high ka region will show the degree of fluctuations to vary much more smoothly in this case as the analysis is performed in a "flat" region, away from any region of strong destructive interference between the specular and Rayleigh surface wave. In this analysis, we explore the problem even deeper by examining the behavior of both the amplitude and phase of the fluctuation component of the scattered signal which will illustrate the behavior of the fluctuations of the echo amplitude.

We begin this part of the analysis by plotting many realizations of $|f|$ as we did in Fig. 4 but now holding ka fixed. Figure 6 illustrates the variations of $|f|/L$ as a function of σ/a for $ka = 0.1$ and 30 which correspond to the Rayleigh and geometric scattering regions. As in Fig. 4, the scattering amplitude is shown to fluctuate more as the roughness increases. One major difference between the plots in this figure and Fig. 4(a) and (b) is that since ka is fixed no oscillatory effect is observed due to interferences between the specular and other waves. Figure 6(a) illustrates how different the nature of the scattering is in the $ka \ll 1$ region than in the $ka \gg 1$ region. While the degree of fluctuations increases with increasing roughness as in the $ka \gg 1$ case, so does the mean field (which *decreases* for $ka \gg 1$). The mean field increases in the $ka \ll 1$ region because variations ζ in local radius cause variations in the local amplitude of the scattered field that are proportional to the *square* of ζ, hence the net increase [Eq. (10)]. Also, the fluctuations always stay small compared with the mean field in the $ka \ll 1$ case. Phase variations of the local scattered field cause a decrease of the mean in the $ka \gg 1$ region [Eq. (19)].

As discussed in Sec. I, the phase of the fluctuation component relative to the mean scattered field must be understood when describing the fluctuations of the echo envelope.

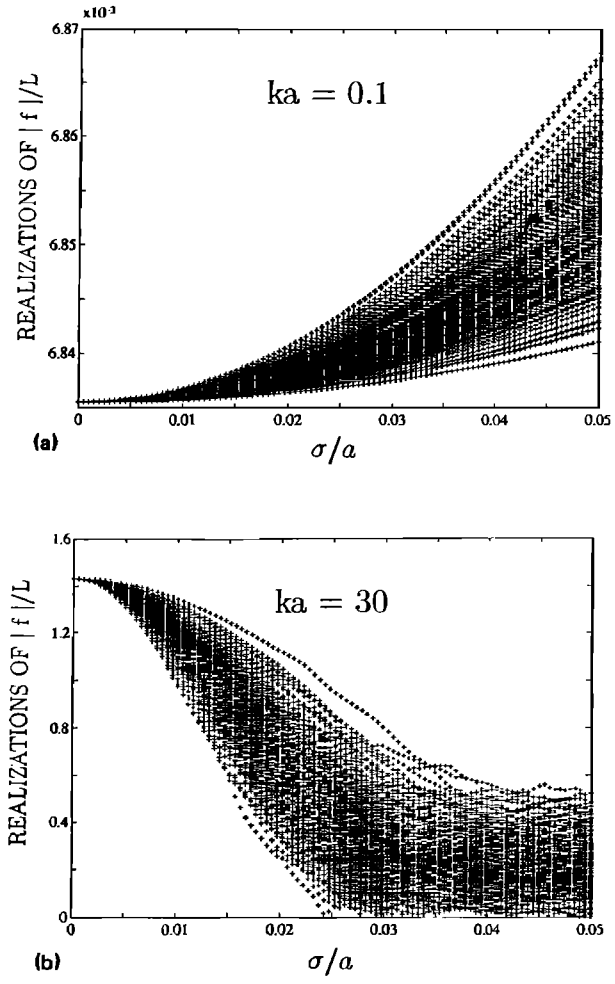

FIG. 6. Realizations of the normalized magnitude of the scattering amplitude or echo envelope, $|f|/L$, plotted for 150 realizations of randomly rough straight finite-length tungsten carbide cylinder at broadside incidence for each value of fractional roughness σ/a. The points were calculated in same manner as in Fig. 4(a) and 4(b) except ka is fixed at values of 0.1 and 30 while σ/a is varied. The fluctuations are shown to be small in the lower extremes of σ/a and increase with increasing σ/a. Fits of the Rice PDF to these data (not shown) are similar to the plots given in Fig. 4(c).

We study the fluctuation component by plotting its (complex) value for an ensemble of realizations. Figures 7 and 8 illustrate distributions of the fluctuation component for different ka and σ/a. Also plotted is the direction of the mean scattered field as indicated by an arrow. The fluctuation component is shown to be narrowly distributed with a phase similar to the mean field in both $ka \ll 1$ and $ka \gg 1$ regions provided $k\sigma \ll 1$ (note that $k\sigma \ll 1$ for all σ/a in the $ka \ll 1$ region). The phase becomes randomly distributed when $k\sigma \gtrsim 1$ in the $ka \gg 1$ region. In the Rayleigh scattering region, the distribution can be explained because the scattering is monopole- and dipolelike and the scattering amplitude and all fluctuations are real [Eq. (9)]. Thus the fluctuations are naturally in phase with the amplitude. In the geometric scattering region, the scattering amplitude is complex. For small $k\sigma$ and σ/a, the components of the variations that are out of phase with the mean field are negligible and hence the fluctu-

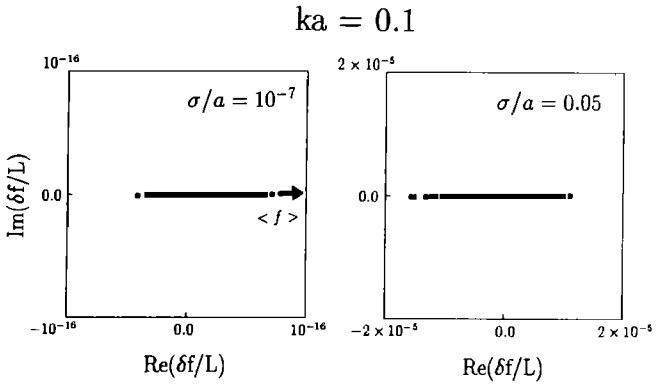

FIG. 7. Fluctuation component, $\delta f = f - \langle f \rangle$, of scattering amplitudes from $ka = 0.1$ plot in Fig. 6 for two values of σ/a. This plot on the complex plane shows the real and imaginary components of δf for 300 realizations at each value of σ/a. Also illustrated is the direction of the mean $\langle f \rangle$ (see arrow). Note that for the sake of illustration, the scale is adapted to the magnitude of δf in each plot. Had the scale remained fixed, δf would have been concentrated in an extremely small area in the lower roughness plot compared with the higher roughness plot. The fluctuation component is shown to have a narrow distribution of phase in phase with the mean scattering amplitude for both roughnesses.

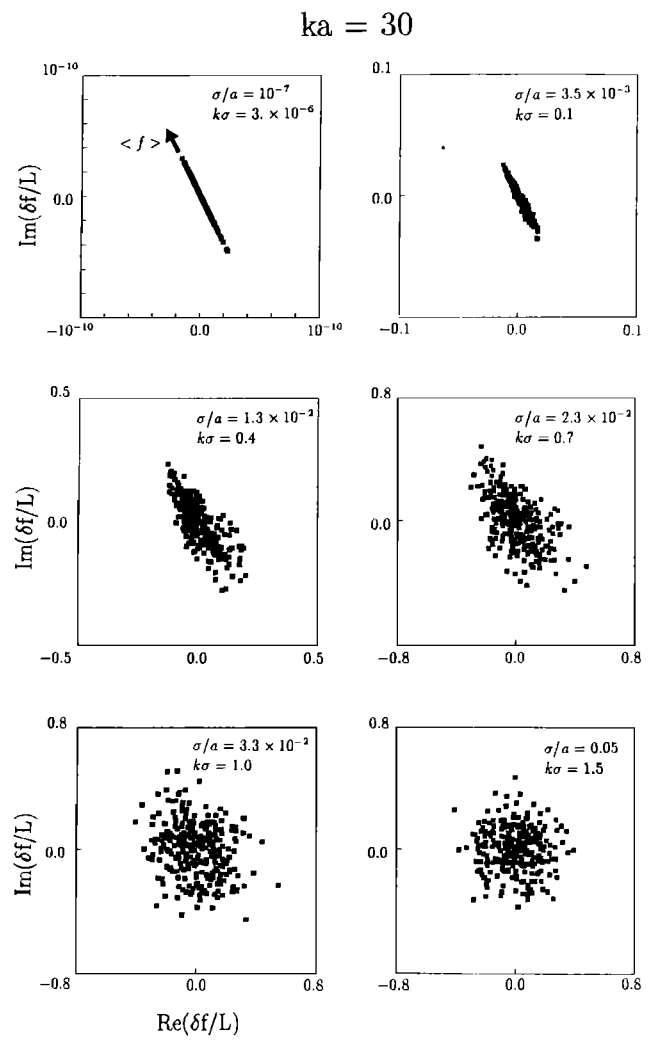

FIG. 8. Same as Fig. 7 but for $ka = 30$ calculations. The distributions are shown to begin narrowly distributed and in phase with the mean scattering amplitude for small σ/a. The distributions become circular as the phase of the fluctuation component becomes randomly distributed for larger σ/a.

ation component is narrowly distributed and in phase with the mean field [Eq. (18)]. When $k\sigma$ becomes larger in the $ka \gg 1$ region, the component of the scattering amplitude that is out of phase from the mean field becomes substantial and the phase of the fluctuation component becomes randomly distributed.

We now examine variations in γ for the above sets of conditions. Figure 9 illustrates plots of γ for fixed values of ka while σ/a is varied. The values of ka and σ/a correspond to those in the study of the fluctuation components in Figs. 7 and 8. In each case, γ is shown to vary inversely with the fourth power of σ/a except in the high roughness region of the $ka = 30$ plot. The curves should be compared with those given in Fig. 5 where γ is constant in the Rayleigh scattering region and deviates from the trend of $(ka)^{-4}$ in the geometric region. In Fig. 9, no such deviations exist as the curves vary smoothly and inversely with the fourth power of σ/a for most or all of the range of σ/a.

Figures 5 and 9 illustrate properties of the scattering by rough volumetric objects that can be compared directly with the case of rough planar interfaces. In the geometric or ray region, the fluctuations depend upon $k\sigma$ for both cases. However, in the Rayleigh scattering region of the volumetric case, the fluctuations are independent of frequency which

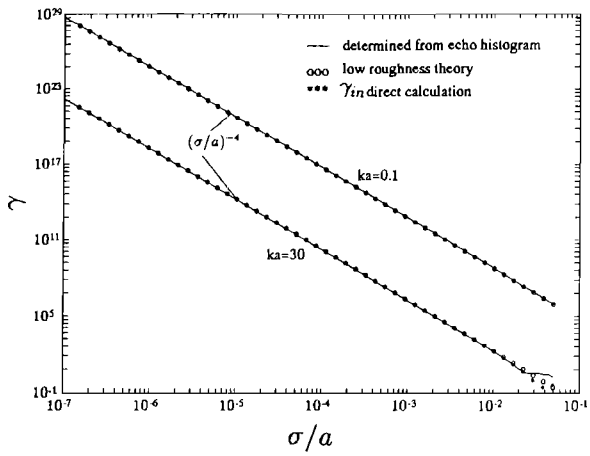

FIG. 9. Rice PDF shape parameter γ plotted against σ/a for $ka = 0.1$ and $ka = 30$. Three-hundred realizations per value of σ/a were used for each value of ka. Parameter extracted two ways from simulations illustrated in Figs. 6–8 and compared with low roughness theory. Solid line represents "observed" or true γ based on simulated fluctuations of $|f|$. (See Fig. 5 caption and text for details on procedure to determine γ.) Asterisks represent γ_{in}, which was *calculated* (no Rice fit was involved) from simulated quantities $\langle f \rangle$ and δf_{in} [Eq. (7)], and open circles represent γ_{in}, which was *calculated* again, but from low roughness theory that ignores all waves but specular [Eq. (15b) for $ka = 0.1$ and Eq. (25) for $ka = 30$]. This figure illustrates the excellent agreement between actual Rice parameter values as determined by simulations of echo envelope and those parameter values calculated either from (a) manipulations of simulated values of scattering amplitude assuming the in-phase fluctuation component dominates the fluctuations and (b) a low roughness theory developed in this article that is based on the monopole and dipole terms in the $ka \ll 1$ region and assumes that the specular component of the echo dominates the trend of the scattering in the $ka \gg 1$ region.

has no counterpart in the case of planar objects. Also, the circumnavigation of the Rayleigh surface elastic wave and interferences of that wave with the specular wave to cause extra variations in γ in Fig. 5 has no counterpart with planar objects.

There is excellent agreement in Fig. 9 between the observed or true γ based on the simulations and the values of γ_{in} based on both direct calculations from the simulated quantities [using Eqs. (5) and (7)] and the approximate low roughness theory given in Eqs. (15b) and (25). The dramatic consistency between all approaches indicates that (1) the fluctuations of the echo envelope are dominated by the in-phase component of the fluctuation component of the scattering amplitude and (2) ignoring all waves except for the specular component provided accurate representation of the trend of the fluctuations in the $ka \gg 1$ region. As one would expect, for high roughness in Fig. 9 ($\sigma/a \gtrsim 0.02$ region in $ka = 30$ plot), γ levels off toward near zero levels (Rayleigh PDF region) and the low roughness theory departs from the observations. This region corresponds to where the phase of the fluctuation component becomes randomly distributed in Fig. 8.

III. COMPARISON WITH EXISTING DATA

While the authors are not aware of any controlled set of data that could properly test the theory presented in this article, it is still useful to compare the results with experimental data that currently exist to help provide insight into real data. There are two interesting sets of data involving the statistics of the echo envelope from marine organisms: (1) Clay and Heist published their analysis of the statistics of the echoes from individual fish under three conditions: calm, moderately active, and wild.[14] In the calm case, the histogram of the echo envelopes was narrow and Gaussian-like while in the active case, the histogram was broad and Rayleigh-like. The PDF took on an intermediate shape in the moderately active case. They found that the Ricean PDF fit the data reasonably well. (2) Wiebe *et al.* analyzed the scattering characteristics of 43 live zooplankton (39 shrimplike crustaceans and 4 gelatinous animals) covering a wide range of sizes at a single frequency.[15] The scattering cross section was analyzed versus length, ka, wet weight, and dry weight. Various scattering models were applied to the data such as the sphere, straight finite length cylinder, and uniformly bent finite-length cylinder to find that the (elongated) organisms behaved acoustically more like elongated targets than spherical ones. The statistical characteristics were also analyzed. Rice PDFs were fit to the data and the characteristics of the Rice shape parameter γ were investigated.

Neither of the above cases obviously represents independent realizations of randomly rough straight elastic cylinders. The fluctuations are due to a combination of changes in both orientation and shape which results in an effective roughness. Because there were more acoustic and morphological data presented by Wiebe *et al.* than by Clay and Heist we will discuss the Wiebe *et al.* data. In fact, the results of this article were applied to the data in the article by Wiebe *et al.* Rather than repeating the analysis, the results of the analysis will be reviewed briefly and for more detail, the reader is referred to that article.

In the analysis presented in the article by Wiebe *et al.*, there was good agreement between the histograms of echo envelope and the Rice PDF. The small organisms, in general, produced narrow PDFs (high γ) with a relatively low mean value of envelope level while the large organisms produced broader PDFs (low γ) with higher mean values. The exceptions to these trends were discussed in that article. This good agreement between the data and theoretical Rice PDFs is consistent with the fact that there is also good agreement between the simulated data in this article and the Rice PDFs.

When plotting the values of γ from the Rice PDF fits versus backscattering cross section, it was found that, in general, γ was inversely proportional to the average backscattering cross section. (The cross section in that article was related to both size and roughness of the shrimp.) The γ-cross section relation was similar, but not identical to that predicted by the theory in this article. Under the conditions of the experiment, one should not expect exact correspondence between a theory which involves straight randomly rough finite-length solid-elastic cylinders at normal incidence and shrimp whose fluidlike body contains an outer elastic shell and both shape and orientation change throughout the data collection. Thus the general trends were more important to compare rather than the details.

In conclusion, the theoretical and simulation results of this article are broadly consistent with the data in the Wiebe *et al.* article where the backscattering by shrimp were involved. Both articles show the echo envelope to obey Ricean statistics with the shape parameter γ varying inversely with some power of backscattering cross section.

IV. CONCLUSIONS

The statistical nature of echoes from randomly rough straight finite-length solid elastic cylinders at broadside incidence was investigated. By use of a limiting form of the modal series solution at $ka \ll 1$ and an approximation of the Sommerfeld–Watson transformation of the modal series solution at $ka \gg 1$ to the infinitely long cylinder as a basis for the deformed cylinder solution, approximate analytical expressions were derived showing the fluctuations to depend upon the wave number (sometimes) of the incident field, the rms roughness, correlation distance of the roughness, and radius of the cylinder. The echo amplitude of the cylinders was found to be approximately Ricean distributed.

There were interesting similarities and differences found between the scattering by volumetric objects such as the cylinders and rough planar interfaces. Similarities: for $ka \gg 1$, the specular component of the scattered field of the cylinder is similar to the specular component of the scattered field due to a rough planar interface. (Note that ray acoustics applies to the scattering by the cylinder in this region.) Differences: also in the $ka \gg 1$ region, there exist surface waves that circumnavigate the cylinder and refracted waves that will be reflected within the boundaries of the interior of the cylinder. Both of these classes of waves eventually reradiate back toward the receiver and affect the nature of the

fluctuations. There is no direct counterpart of these waves in the problem of scattering by rough planar interfaces although certainly such waves can exist under some conditions: (1) a single path of surface waves that will reradiate in the specular direction and (2) multiply reflected waves in a layered medium below the rough interface. (Note that multiply internal reflected waves in a cylinder can exist for a homogeneous, nonlayered material.) In the $ka \ll 1$ or Rayleigh scattering region, there is also a difference. In this region, the degree of fluctuations becomes independent of frequency for all ranges of roughness—a phenomenon that does not exist in the subject of the scattering by rough planar interfaces. (Certainly in the high roughness region of planar interfaces, all fluctuations become Rayleigh distributed and independent of frequency, but the fluctuations are strongly dependent upon frequency in the low roughness region.) All of the above-mentioned differences between the fluctuations of the scattered field from rough cylinders and rough planar interfaces are due to the fact that volumetric objects such as cylinders are bounded and planar interfaces are not.

It was also shown in this article that the phase of the fluctuation component of the scattered field (where the component is sometimes referred to as the "incoherent" term) was sometimes narrowly distributed. This distribution needed to be taken into account when describing the statistical behavior of the echo envelope.

Finally, the predictions based on this analysis of the straight rough finite cylinders were compared in another article with data involving backscattering from live zooplankton and it was found that the predictions were broadly similar to the scattering characteristics of the animals. It was obvious from the comparisons that in order to adequately describe the statistical nature of the fluctuations of the echoes from naturally occurring objects such as marine organisms, more complex shapes and orientation need to be taken into account. The deformed cylinder solution is capable of describing the more complex shapes and orientation. The challenge lies in gathering accurate morphological and behavioral information so that accurate predictions can be made.

ACKNOWLEDGMENTS

The authors are grateful to the following people from the Woods Hole Oceanographic Institution, Woods Hole, MA: Bob Eastwood for his aid in the numerical computations on the computer and Shirley Bowman for preparing the manuscript to this article. This work was supported by the U.S. Office of Naval Research Grant Nos. N00014-89-J-1729 and N00014-90-J-1804. This is Woods Hole Oceanographic Institution Contribution Number 7743.

APPENDIX: ERRORS INDUCED BY USE OF NONZERO MEAN ROUGHNESS IN SIMULATIONS

When generating the randomly rough surfaces for the numerical simulations, it would be ideal for the roughness component of each surface to have a zero mean both with respect to z integration ($\int \zeta\, dz = 0$) and ensemble of surfaces ($\langle \zeta \rangle = 0$) as assumed in the theory. Since the two conditions cannot be simultaneously met, unwanted effects arise in the simulations.

Certainly, an infinite number of infinitely long surfaces will have negligibly small means when constructing the surfaces out of summations of random phase, random frequency sinusoids as described in Ref. 1. However, for a finite number of finite-length surfaces that are sampled discretely for the purpose of the computer simulations, the means may not be sufficiently close to zero and the surfaces must be adjusted accordingly to at least partially compensate for the offset. Since more surfaces were used than number of samples or integration points per surface, the ensemble means $\langle \zeta \rangle$ in our analysis in the main text appeared to be sufficiently small for the purpose of numerical simulations while each surface needed to be adjusted via an offset level so that the integral $\int_{-L/2}^{L/2} \zeta\, dz = 0$ for each surface. The surfaces could not be adjusted so that the statistical means $\langle \zeta \rangle$ for all z were simultaneously equal to zero.

When the surfaces are not adjusted, the integral $\int_{-L/2}^{L/2} \zeta\, dz$ will be nonzero and the echo fluctuations will behave in a manner dramatically different under some conditions than described in the main text where the integral was equal to zero. For sufficiently small σ/a, the small but finite value of the integral allows a term $(\sigma/a)^2$ to dominate γ. Had the integral been zero, this term would not exist and the higher-order term $(\sigma/a)^4$ would prevail for all small σ/a as shown in the main text.

The above effects are illustrated in Figs. A1 and A2. Figure A1 illustrates the dramatic effect the nonzero mean surface has on the fluctuation component δf in the geometric scattering region ($ka = 30$). When the surface is adjusted so $\int \zeta\, dz = 0$, δf is in phase with the mean amplitude $\langle f \rangle$ while before the surfaces have been adjusted and $\int \zeta\, dz \neq 0$, it is 90° out of phase of $\langle f \rangle$. The effect this phenomenon has on the fluctuations of the echo envelope is illustrated in Fig. A2 where γ is plotted versus σ/a for both the adjusted and nonadjusted surfaces. For the calculations involving the adjust-

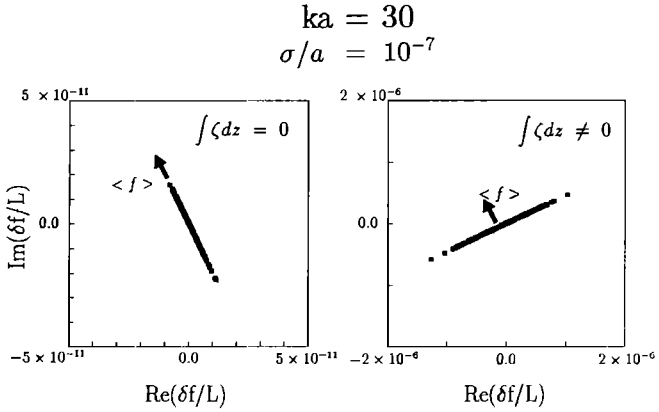

FIG. A1. Fluctuation component for the cases of "adjusted" surfaces so that $\int \zeta\, dz = 0$ and nonadjusted surfaces so that $\int \zeta\, dz \neq 0$. The narrowly distributed phase in each case is shown to depend dramatically on whether or not the average roughness along the length of the cylinder is equal to zero. Three-hundred realizations were used in each case. The direction of the mean scattering amplitude $\langle f \rangle$ is given by the arrow: $ka = 30$ and $\sigma/a = 10^{-7}$.

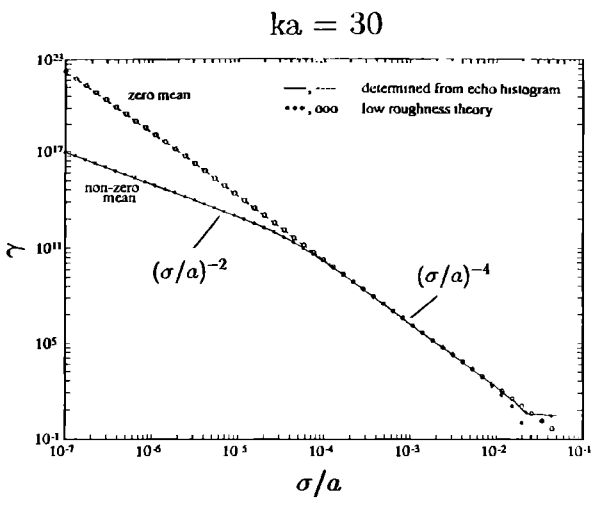

FIG. A2. Values of γ for $\int \zeta\, dz = 0$ and $\int \zeta\, dz \neq 0$ surfaces for fixed ka as σ/a varies. Procedure to determine γ from echo histogram is given in caption to Fig. 5, the zero mean theory is given in Eq. (25), while the nonzero-mean theory (not given) is based on a derivation similar to that leading up to Eq. (25), but assuming that the roughness has a nonzero mean along the length of the cylinder. Three-hundred realizations per value of σ/a were used to generate each set of points. The curves are shown to deviate substantially from each other for small σ/a illustrating the importance of adjusting the surfaces so that their roughness has a zero mean along the length.

ed surfaces, γ is shown to vary as $(\sigma/a)^{-4}$ for all small σ/a. Calculations involving the nonadjusted surfaces predict that γ will deviate from the adjusted surface calculations for very small σ/a by varying as $(\sigma/a)^{-2}$. As discussed above, this effect is due to the fact that for very small σ/a, the $(\sigma/a)^2$ factor to the integral $\int \zeta\, dz$ dominates the variations. [The derivation of our equation (not given) predicting this behavior is similar to the one in the main text leading up to Eq. (25) with the exception of $\int \zeta\, dz$ being held nonzero.] It is also interesting to note that regardless of whether we use adjusted or nonadjusted surfaces, γ_{in}, as calculated with Eq. (7) (not shown), coincides with the γ observed in the corresponding case. Since Fig. A1 shows δf to follow dramatically different trends in the two cases, the fact that γ_{in} follows each set of observations demonstrates the importance of the in-phase component of the fluctuation component to the echo envelope fluctuations.

In conclusion, in order to avoid errors in describing the echo fluctuations in the very low roughness region, it is important to adjust the simulated rough surfaces for these finite-length objects so that the average value of the roughness across the length of the surface is zero. Since the surfaces cannot be adjusted so that $\langle \zeta \rangle = 0$ for all z simultaneously, caution should be taken when performing simulations.

[1] T. K. Stanton, "Sound scattering by rough elongated elastic objects. I. Means of scattered field," J. Acoust. Soc. Am. **92**, 1641–1664 (1992).

[2] S. O. Rice, "Mathematical analysis of random noise," in *Selected Papers on Noise and Stochastic Processes*, edited by N. Wax (Dover, New York, 1954), pp. 133–294.

[3] J. W. Goodman, *Statistical Optics* (Wiley, New York, 1985), pp. 50–55.

[4] T. K. Stanton, "Sonar estimates of sea floor microroughness," J. Acoust. Soc. Am. **75**, 809–818 (1984).

[5] R. S. Hoyt, "Probability functions for the modulus and angle of the normal complex variate," Bell Syst. Tech. J. **26**, 318–359 (1947).

[6] K. L. Williams and P. L. Marston, "Backscattering from an elastic sphere: Sommerfeld-Watson transformation and experimental confirmation," J. Acoust. Soc. Am. **78**, 1093–1102 (1985).

[7] K. L. Williams and P. L. Marston, "Synthesis of backscattering from an elastic sphere using the Sommerfeld–Watson transformation and giving a Fabry–Perot analysis of resonances," J. Acoust. Soc. Am. **79**, 1702–1708 (1986).

[8] K. L. Williams and P. L. Marston, "Scattering from an aluminum sphere: Fabry–Perot analysis of resonances based on the Watson transformation," in *Proceedings of the 12th International Congress on Acoustics* (Beauregard, Toronto, 1986), pp. I1-2.1-2.

[9] P. L. Marston, "GTD for backscattering from elastic spheres and cylinders in water and the coupling of surface elastic waves with the acoustic field," J. Acoust. Soc. Am. **83**, 25–37 (1988).

[10] C. Eckart, "The scattering of sound from the sea surface," J. Acoust. Soc. Am. **25**, 566–570 (1953).

[11] J. M. Proud, Jr., R. T. Beyer, and P. Tamarkin, "Reflection of sound from randomly rough surfaces," J. Acoust. Soc. Am. **31**, 543–552 (1960).

[12] C. S. Clay and H. Medwin, *Acoustical Oceanography: Principles and Applications* (Wiley-Interscience, New York, 1977).

[13] T. K. Stanton, "Sound scattering by cylinders of finite length II. Elastic cylinders," J. Acoust. Soc. Am. **83**, 64–67 (1988).

[14] C. S. Clay and B. G. Heist, "Acoustic scattering by fish-acoustic models and a two parameter fit," J. Acoust. Soc. Am. **75**, 1077–1083 (1984).

[15] P. H. Wiebe, C. H. Greene, T. K. Stanton, and J. Burczynski, "Sound scattering by live zooplankton and micronekton: empirical studies with a dual-beam acoustical system," J. Acoust. Soc. Am. **88**, 2346–2360 (1990).